Digital SCAL in Complex Carbonates by the Density Functional Hydrodynamics Method

Denis Klemin[1], *Shehadeh Masalmeh*[2], *Ali AlSumaiti*[2], *Ritesh Bhakta*[1], and *Moustafa Dernaika*[3*]

[1]SLB, Reservoir Performance Evaluation, Houston, Texas, USA
[2]ADNOC HQ, Upstream, EOR Department, Abu Dhabi, UAE
[3]SLB, Reservoir Performance Evaluation, Abu Dhabi, UAE

Abstract. Pore-scale modelling has seen tremendous development with increasing imaging and data processing capabilities as well as associated advancement in the description of the physics of multi-phase flow at pore scale and related computational algorithms. As a result, the digital SCAL technology is finding increasing application to understand petrophysical rock properties and to reduce reservoir characterization uncertainties where experimental measurements on core samples may be lacking. The aim of this work was to validate and verify the accuracy of the Density Functional Hydrodynamics (DFH) Method in predicting reliable relative permeability data in mixed-wet carbonate reservoir rock types. Four plugs were selected to represent dolomite and limestone rock types from an offshore field in Abu Dhabi. The samples' porosity and permeability values ranged from 0.14 to 0.30 (fractional) and from 40 mD to 60 mD, respectively. The following workflow was implemented to obtain representative 3D digital rock models (DRMs):

- Plug-scale X-ray CT at a resolution of 50x50x300 micron/voxel (X, Y, Z) to assess the plug heterogeneity and to aid in selecting representative subsamples for higher resolution scanning and MICP analysis.
- Selection and cutting of the subsample as a (4mmx15mm) cylindrical mini-plug.
- MicroCT of the mini-plug at around 1 micron/voxel resolution.
- High resolution SEM Mosaic imaging at 100nm/pixel on ion-milled surfaces of the mini-plug and sample mineralogy classification with EDS AMICS analysis.
- Construction of multi-scale 3D digital rock model (DRM) from the microCT and the SEM data.

Capillary pressure and relative permeability curves were simulated in the DRM by the direct modelling method that was implemented in Direct Hydrodynamic (DHD) simulator. The method employs a diffuse interface approximation at fluid/fluid boundaries with Helmholtz energy-based thermodynamic model. The simulation uses classical mass, momentum, and energy conservation laws with constitutive relations ensuring consistency between hydrodynamic and thermodynamic descriptions of multiphase compositional systems in the frame of the density functional approach, which allows complex flow processes to be modelled.

Porosity, permeability and MICP data were obtained from simulation in the multi-scale constructed DRMs, which compared reasonably well with the unimodal and bimodal pore-throat size distributions of the studied plug samples. This comparison was vital to validate the DRMs and to confirm that the digital rocks captured accurately the pore system properties of the samples. Wettability input into the rock model was distributed as contact angles between the fluid pair and the rock surface. The distribution of the wettability was constrained by the experimental drainage and imbibition capillary pressure properties of the samples. Waterflood relative permeability curves were predicted in the validated DRMs with assigned saturation-driven mixed wettability using the DHD simulator. The digital curves compared very well with the experimental measurements performed on the corresponding SCAL plugs.

This work was part of a validation and verification project to better understand Digital SCAL by the DFH method. The study ran on a blind test basis, where the experimental relative permeability curves were not disclosed until after the pore-scale simulations were reported. The DFH modelling technology offers a great opportunity to provide digital SCAL as a complementary approach to conventional SCAL, which will help reduce cost and fill gaps in complex flow scenarios such as Enhanced Oil Recovery

1 Introduction

Digital Rock Physics (DRP) has undergone transformative advancement over the past two decades, driven by significant progress in high-resolution imaging (e.g., micro-CT), sophisticated data processing, enhanced

* Corresponding author: mdernaika@slb.com

computational algorithms, and a deeper understanding of pore-scale multiphase flow physics. This evolution positions DRP, or "digital SCAL" as a powerful tool for characterizing petrophysical properties and reducing reservoir uncertainty, particularly where conventional core analysis (SCAL) data is limited.

Despite these advancements, the *a priori* predictive capability of DRP for fundamental two-phase flow properties – specifically relative permeability and capillary pressure curves – remains challenging, especially for complex rock-fluid systems like mixed-wet carbonates. Key challenges persist:

1. **Wettability Representation:** Accurate prediction requires detailed knowledge of pore-scale wettability distribution, which cannot be derived solely from rock images.
2. **Network Generation:** Extracting representative pore network models (PNMs) from images remains non-trivial and often lacks sufficient constraint.
3. **Modeling Physics:** Traditional approaches, particularly quasi-static PNMs, exhibit limitations in accurately capturing the complex physics of multiphase displacement dynamics.

Consequently, current DRP workflows cannot reliably predict two-phase properties based exclusively on image data. Predictions are often contingent upon unverified assumptions regarding wettability distribution and network structure, leading to results whose representativeness is intrinsically linked to the validity of these assumptions rather than the true rock-fluid system.

This study directly addresses these challenges by presenting a comprehensive workflow to validate and enhance the predictive capability of DRP, specifically employing the Density Functional Hydrodynamics (DFH) Method [1, 2]. The primary objectives are:

1. **Validation:** To rigorously verify the accuracy of the DFH method in predicting reliable relative permeability data for complex mixed-wet carbonate rocks.
2. **Workflow Development:** To outline a robust methodology for overcoming core DRP limitations, focusing on:
    - Generating representative pore networks anchored by experimental drainage capillary pressure curves.
    - Demonstrating the DFH method's ability to accurately capture pore-scale fluid flow physics.
    - Calibrating pore-scale wettability distributions using experimental SCAL data to ensure representativeness.

Four plugs were selected for this study to represent dolomite and limestone rock types from an offshore field in Abu Dhabi. These plugs were used in digital rock analysis (DRA) workflow that combines experimental and numerical studies helping to evaluate fluid transport and petrophysical properties at pore scale. The process involved imaging the core samples using X-ray computed tomography (CT) and microcomputed tomography (MicroCT), complemented by scanning electron microscopy (SEM), to create digital rock (DR) models that capture the complex pore structures of the studied rocks. It also included generating digital representations of reservoir and injection fluids and performing pore-scale simulations of multiphase flow using the DFH Method within the Direct Hydrodynamic (DHD) simulator. The method employs a diffuse interface approximation at fluid/fluid boundaries with Helmholtz energy-based thermodynamic model. The simulation uses classical mass, momentum, and energy conservation laws with constitutive relations ensuring consistency between hydrodynamic and thermodynamic descriptions of multiphase compositional systems in the frame of the density functional approach, which allows complex flow processes to be modelled [1].

The DFH modelling technology allows to effectively reduce time required for Special Core Analysis (SCAL) long-duration laboratory core tests using the Digital SCAL experiments It can also complement conventional SCAL program [3-5], to reduce cost and fill gaps in complex flow scenarios such as Enhanced Oil Recovery [6-7]. This work is part of a validation and verification project to better understand Digital SCAL by the DFH method. The study ran on a blind test basis, where the experimental relative permeability curves were not disclosed until after the pore-scale simulations were reported.

2 Core Material

Four carbonate rock samples representing dolomite and limestone rock types from an offshore field in Abu Dhabi were selected for the study. Each sample was CT scanned (Figure 1) at a resolution of 50x50x300 micron/voxel (X, Y, Z) to assess plug heterogeneity, select plugs for the Digital SCAL study, and aid in selecting representative subsamples for higher resolution scanning and MICP analysis. Sample #4 and #18A are dolomite, while #12 and #23A are limestone rocks.

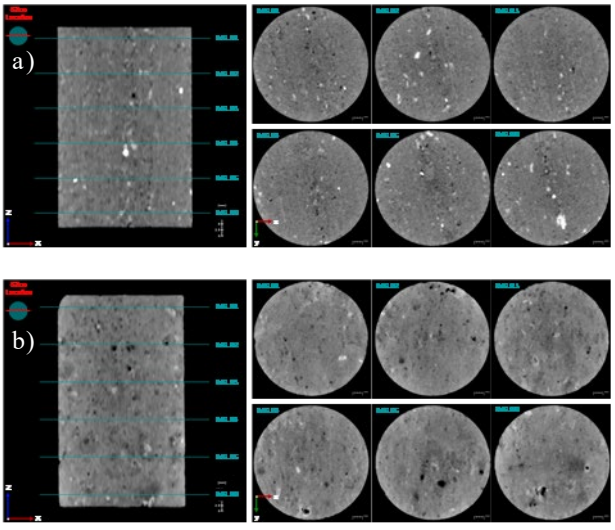

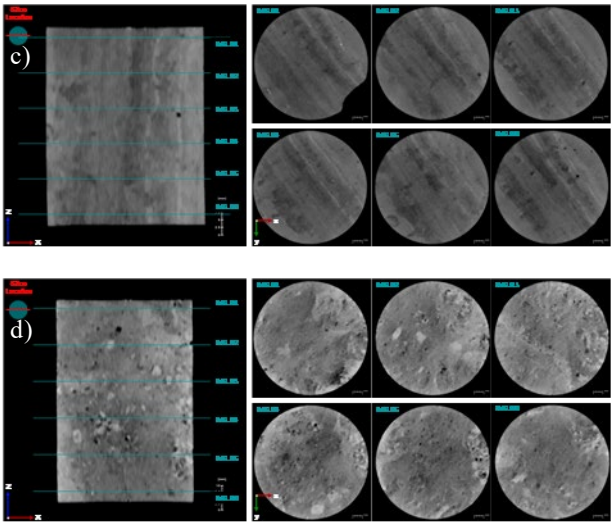

Figure 1. CT scanning data on a) sample 4, b) sample 12, c) sample 18A, d) sample 23A.

3 Physical Measurements

Physical rock measurements including scanning of the core material, provide necessary input data for the digital rock models. Multiscale imaging was performed on the samples and included computed tomography (CT), high-resolution microCT imaging and scanning electron microscopy (SEM). Sample routine properties were measured (Table 1). The samples' porosity and permeability values ranged from 0.14 to 0.30 (fractional) and from 40 mD to 60 mD, respectively. Other data obtained included mercury injection capillary pressure (MICP) tests on all the samples, which were used to QC the constructed DR models, and Advanced Mineral Identification and Characterization System (AMICS), which helped confirm sample minerology.

Table 1. Routine core analysis data on studied samples.

Sample ID	Gas Permeability @ Ambient (mD)	Klinkenberg Permeability @ Ambient (mD)	Porosity @ Ambient, %	Grain Density, g/cm3
4	67.59	61.31	14.40	2.86
12	47.91	42.56	28.56	2.71
18A	64.04	57.11	29.67	2.84
23A	67.68	61.35	16.78	2.71

4 Digital Workflow

4.1 Construction of the digital rock model

Plug imaging data was analyzed, and subsampling locations were selected for mini-plugs to perform higher resolution imaging (Figure 2). Every subsample was carefully selected to represent average CT data of the mother plug 3D image. The subsampling location selection process included multiple steps. A CT scan was performed on the entire rock sample to reveal its internal structure. This initial scan allows the identification of density and textural heterogeneities. Density variations are indicative of differences in the porous medium, while textures provide insights into the rock's geological history and diagenesis. By modeling these intrinsic properties, we generated a 3D analysis of the sample's flow units, allowing us to identify the preferential flow regimes within the sample. Based on this, we strategically select the optimal number and locations of subsamples for subsequent, high-resolution pore-scale imaging to ensure the capture of dominant flow units and accurate representation of the entire flow network.

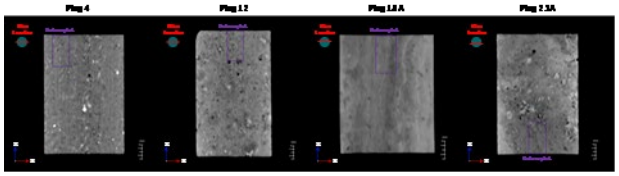

Figure 2. CT scanning data and subsample locations (purple box) for high resolution MicroCT imaging.

During the next step, samples were trimmed, leaving most of the plug material intact. The trims were subsampled to acquire cylindrical mini-plugs of 3-5 mm in diameter by 1.3 cm in height for high resolution MicroCT imaging (an exemplary schematic portraying the subsampling process is shown in Figure 3). High-resolution microCT plug scanning was performed with a Zeiss Xradia Versa 520 micro-CT scanner.

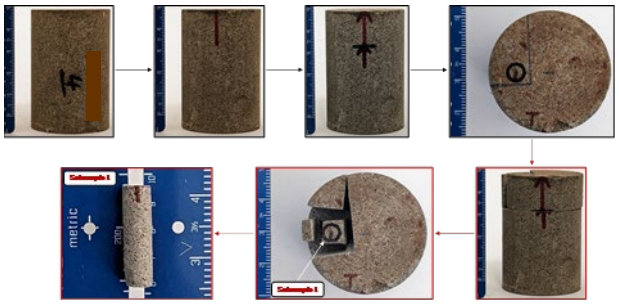

Figure 3. Schematic portraying the subsampling process for sample 4.

X-ray microCT scanning provides a micrometer-scale resolution image of pore spaces within the rock. The core mini-plugs were imaged with the microCT scanner at a high resolution of 1.4564 micron/voxel for sample 4, 1.2578 micron/voxel for samples 12, 18A, and 23A. The scan data was then used to visualize core grains and microCT resolved porosity (Figure 4). High resolution X-ray microCT scanning provided micron-scale resolution that permitted sample structure visualization.

For SEM imaging the subsample was cut through the middle along the main axis of the sample mini-plug. SEM samples were prepared using cut core mini-plugs mounted on an aluminum SEM stub as a polished round. The polished round was milled for 4-8 hours in a Fischione Model 1060 SEM Argon Ion Mill to ensure a horizontal, flat, and polished surface optimal for high magnification SEM imaging. The polished round was sputter-coated for 30 seconds with platinum/palladium to reduce charging artefacts that result from a build-up of electrons on the

sample surface. Samples were then placed in a FEI Quanta 650 FEG field emission scanning electron microscope (Figure 5). SEM imaging started with acquiring a medium resolution (200 nm per pixel or less) overview mosaic image covering a mini-plug sample area.

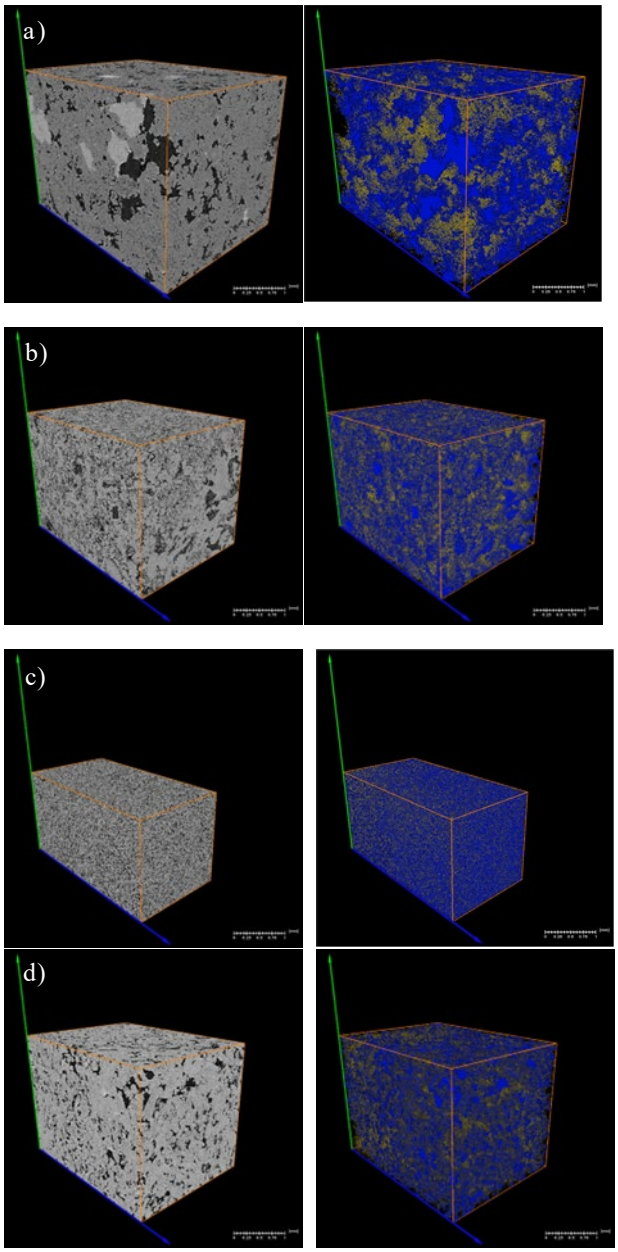

Figure 4. High resolution MicroCT imaging data and digital rock models: a) sample 4, b) sample 12, c) sample 18A, d) sample 23A subsample 2, where MicroCT resolved porosity is shown in blue color, submicron porosity is shown in yellow colour.

SEM imaging then continued with acquisition of 2D high-resolution SEM mosaic images captured in backscattered electron (BSE) mode. High-resolution SEM imaging was executed at 100 nm per pixel covering area of approximately 4.5 x 4.5 mm. The high-resolution SEM imaging data is shown in Figure 5. The SEM data provided an input to submicron porosity identification and quantification for the MicroCT dataset. SEM site location was registered within MicroCT dataset and used to define porosity values in voxels with submicron porosity. Image registration data allowed to define functional dependency between greyscale values and submicron porosity that was then used to construct digital rock models as shown in Figure 4.

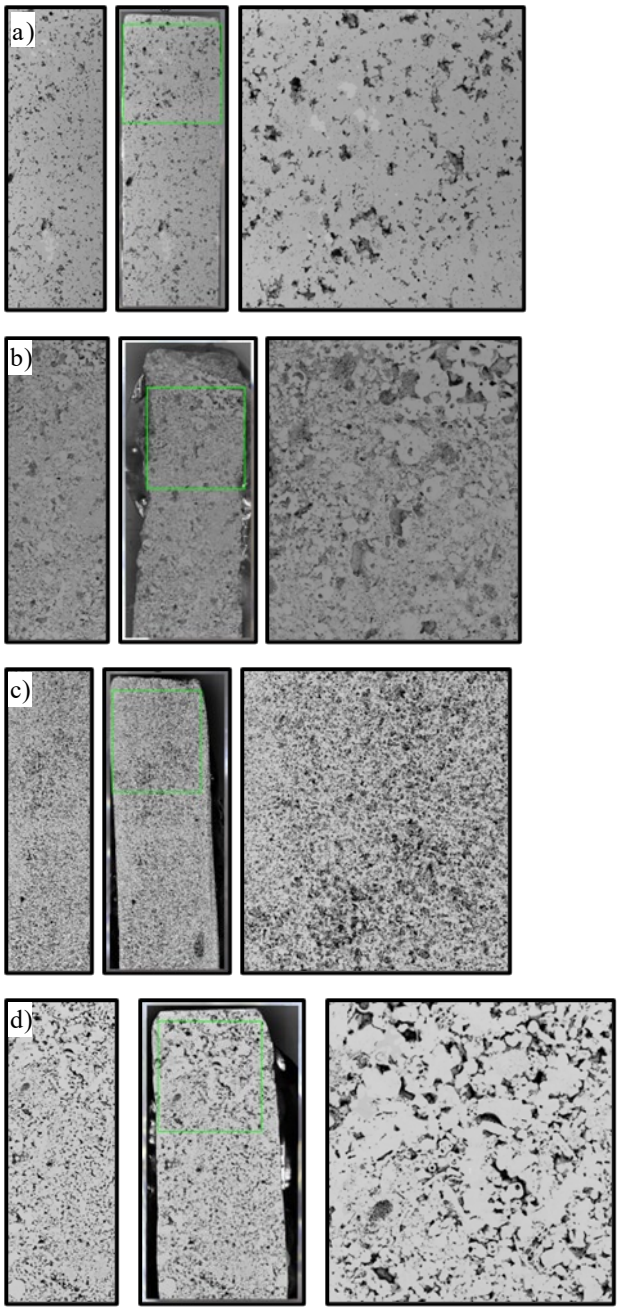

Figure 5. Left to right: medium resolution SEM mosaic imaging (200 nm/pixel), high resolution imaging location (in green), high resolution SEM mosaic imaging (100 nm/pixel): a) sample 4, b) sample 12, c) sample 18A, d) sample 23A.

AMICS mineralogical analysis was conducted on each sample. Sample areas corresponding to high resolution SEM images were used for AMICS mineralogical analysis for all samples. Results include an overview of SEM image of the analyzed area, detailed classification maps for studied mineral instances performed at 500 nm/pixel resolution to reveal sample mineralogical composition. Results provide information on sample matrix composition, micro-textures, clay minerals, detrital grains, and diagenetic minerals and were used to

finalize DR subsample selection and plan the DR modelling program. Overview BSE maps and AMICS mineralogical maps are shown in Figure 6.

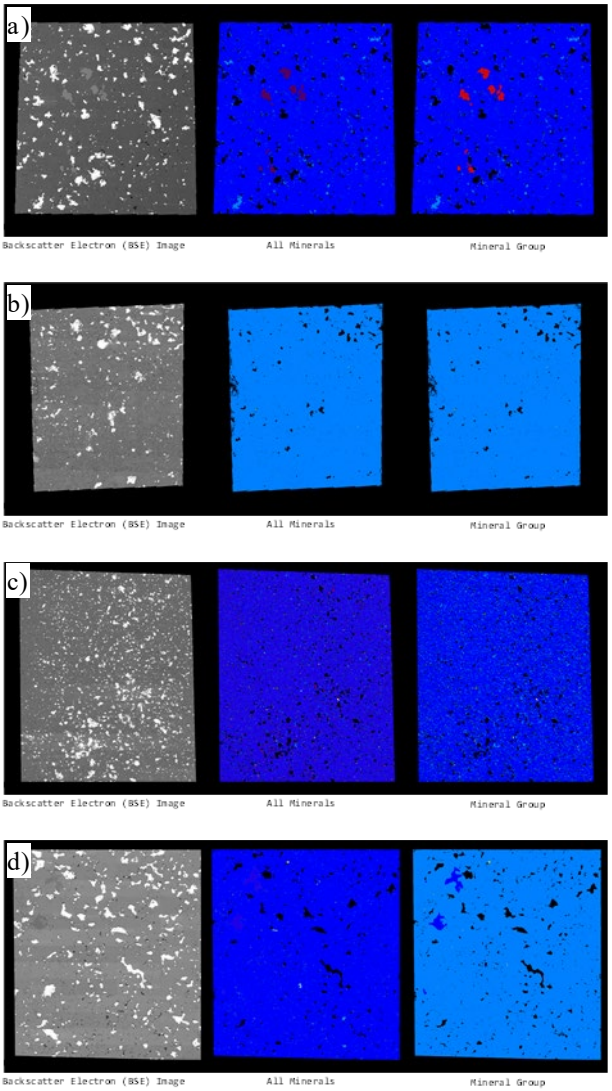

Figure 6. AMICS mineralogical analysis data - left to right: overview BSE SEM image of the analyzed area, detailed classification maps for studied mineral instances and grouped minerology maps for a) sample 4, b) sample 12, c) sample 18A, d) sample 23A.

Summary of mineralogical composition from AMICS is shown in Table 2. AMICS analysis reveals a similar mineralogical composition between samples 4 and 18A. Samples 12 and 23A have different mineralogical content. Samples 4 and 18A are dominated with dolomite (96 – 86%) and with lower calcite content (2.6 – 13%) and contain non-significant amounts of silicates (0.18 – 0.87 %) and clays (0.01%). Samples 12 and 23A have non-significant amount of dolomite (1%) and almost 99% of calcite, mineral weight fractions of silicates and clays are equal to 0.1% and 0.02% respectively.

The digital rock models of the 4 studied samples were built from shadow projections of X-ray microCT and corresponding high-resolution SEM data. These models were shown in Figure 4 (right) with resolved porosity in blue color and submicron porosity in yellow color. The method includes 2D cross-sections reconstruction for each mini plug scan with voxel size equivalent to the microCT resolution, regularization, segmentation, and conversion to a rock model.

Table 2. Summary of mineralogical composition from AMICS.

Modal Mineralogy EDS AMICS analysis							
Sample ID	Quartz	Calcite	Dolomite	Anhydrite	Biotite	Illite/ Mica	Chlorite
	wt %	wt %	wt %	wt %	wt %	wt %	wt %
4	0.18	2.63	96.16	1.03	0	0	0
12	0.06	99.52	0.4	0	0	0.02	0
18A	0.87	13.13	85.97	0	0.01	0	0.01
23A	0.1	98.84	1.04	0	0	0.02	0

4.1.1 Validation of the model

Each constructed digital rock model was verified using laboratory data obtained on the original plug. Permeability was determined by simulation of gas flow through the digital rock model using DHD simulator. The deliverable is a table containing porosity and axial permeability values for each digital rock model. Porosity and permeability data for the digital samples 4, 12, 18A and 23A are listed in Table 3. The percent difference in permeability between simulated and measured values is less than 3%, except for sample #18A, which gives 11%. Porosity difference is less than 0.5 porosity unit.

Table 3. Digital routine core analysis data on studied samples

Sample ID	DR Gas Permeability (mD)	DR Porosity, %
4	65.60	14.58
12	47.71	28.4
18A	71.33	29.35
23A	66.73	16.5

Following permeability and porosity validation, the digital rock model pore structure was verified using laboratory MICP data. Laboratory MICP sample was trimmed from the same 1.5" diameter mother plug adjacent to the mini-plug used in digital imaging. Thickness of the MICP trim was around 5 mm, and was analysed for helium porosity to ensure it matched corresponding core plug within ±2% porosity units. The derived digital mercury injection data were used to attain the mercury-air capillary pressure curve and pore throat size distribution of the constructed digital rock model. Obtained digital data was compared with physical MICP experiment. Mercury-air capillary pressure and pore throat size distribution are shown in Figure 7. Good match between laboratory and digital MICP data was observed on all studied samples. The validation process was a crucial step for obtaining digital rock models that are representative of the pore structure of the different samples under study. For example, sample 23A was subsampled twice to account for the sample heterogeneity (i.e., bimodal distribution) and to capture accurately the pore-throat size distribution as depicted in figure 7

(Digital 23A). Detailed multi-scale analysis was performed to improve the match between digital and physical MICP curves. It is, therefore, important, that we follow a hybrid approach to use experimental data together with digital simulation to ensure that the digital sample is an accurate representation of the rock pore system. Sample #4 shows discrepancy between the physical and digital Pc data around 60% mercury saturation. This difference could be due to unrepresentative selection of either the physical or digital sample. Sample #4 was not selected for Digital SCAL in this study; hence this discrepancy shall be investigated in future work.

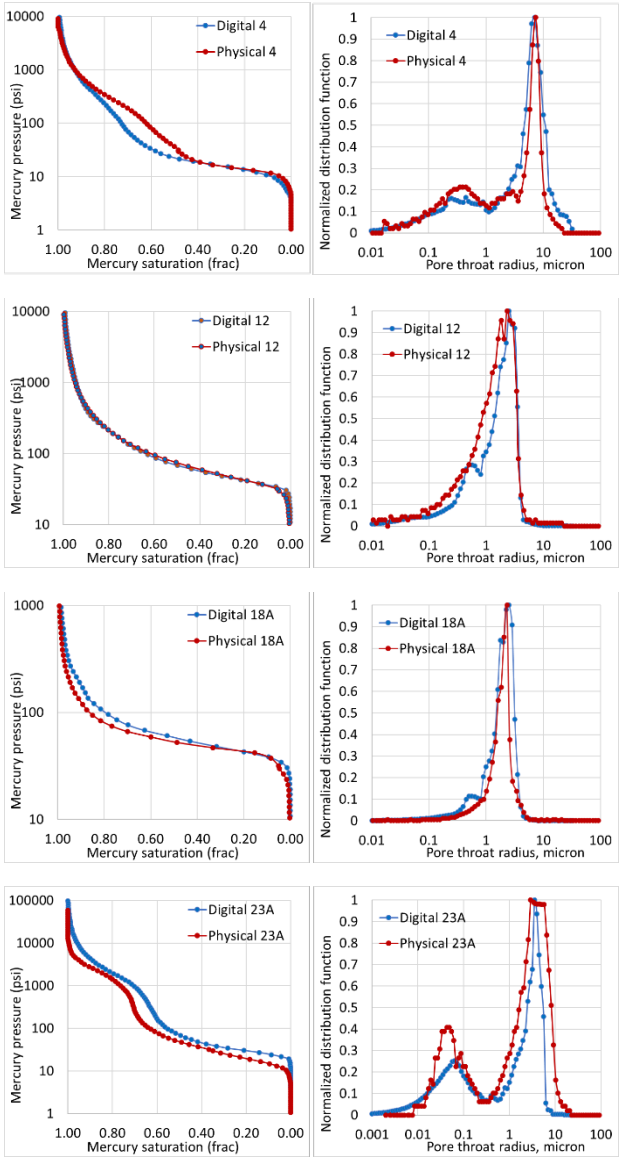

Figure 7. Mercury pressure versus mercury saturation (left) and pore throat radius distribution (right) curves from digital simulation and physical MICP experiments for all the samples. Legends give sample number, digital and physical data.

Porosity, permeability and MICP data were obtained from simulation in the multi-scale constructed DRMs, which (at the end) compared reasonably well with the unimodal and bimodal pore-throat size distributions of the studied plug samples. This comparison was vital to validate the DRMs and to confirm that the digital rocks captured accurately the pore system properties of the samples. Samples 18A (dolomite) and 23A (limestone) were selected for further Digital SCAL (DSCAL) analysis including capillary pressure and relative permeability computations as the most representative of their respectful rock textures.

4.2 Wettability

Multiphase fluid flow properties are highly influenced by the wettability of the porous medium. Therefore, in addition to constructing a representative 3D rock model based on multiscale imaging, wettability must be independently measured, as it is a critical input for accurately predicting two-phase flow behaviour. Wettability input into the rock model is distributed as contact angles between the fluid pair and the rock surface. The following workflow is performed to assign sample wettability: samples are initially saturated with water. During the following sequential floodings, phase saturation and capillary pressure were monitored. During the multiphase modelling, portions of rock surfaces in contact with oil during the drainage cycle exhibit a change in contact angle to 105° (in the current study) while other surfaces remained at original wetting conditions, rendering samples mixed wet. This distribution of the wettability was constrained by experimental drainage and imbibition capillary pressure properties following the workflow in [8] and by deriving advancing contact angle as described in the work of Masalmeh and Jing [9].

4.3 Pore-scale simulation

Capillary pressure and relative permeability curves were simulated in the DRMs by the DFH method that was implemented in Direct Hydrodynamic (DHD) simulator. This method combines classical thermodynamics and hydrodynamics via constitutive relations with particular expression for the density functional that is based on Helmholtz energy of multiphase multicomponent system. The system of equations is the same everywhere and phase interfaces are treated by means of diffuse-interface approach. Density functional theory (DFT) central idea is representation of energy of a heterogeneous system as a functional of densities of chemical components constituting this system.

DFT applications in hydrodynamics of multiphase compositional mixtures was first developed by Dinariev in 1995 [2]. DFH uses classical mass, momentum, and energy conservation laws with specific constitutive relations. These constitutive relations are derived to ensure consistency between hydrodynamic and thermodynamic descriptions of multiphase compositional system in the frame of the density functional approach. The specific expression for the density functional uses square gradients of molar densities, which enables description of surface tension. The thermodynamic state of the mixture is described by means of bulk and surface

Helmholtz energies, where the latter enables correct description of liquid-solid interaction, i.e., wettability and adsorption. The primary variables are molar densities of chemical components, mass velocity of the medium, and internal energy density.

The dynamic combination of digital rock and fluid models occurs in the direct hydrodynamic pore-scale flow simulator, DHD. The DHD is a multiphase compositional hydrodynamic simulator that is based on the Density functional hydrodynamics (DFH). DHD has the ability to handle complex fluids, including surfactant and polymer solutions, complex compositional fluids with phase transitions (including miscible and immiscible gas injection). DHD simulator is the general-purpose pore-scale simulator that enables detailed routine core analysis (RCA), special core analysis (SCAL), and enhanced oil recovery (EOR) agent optimization using a combination of digital representation of the pore structure, detailed digital fluid model of reservoir fluids and injectants, and rock-fluid interaction.

We followed the novel approach suggested by Dinariev et al., 2019, in which transport in small-size pores (e.g., SEM submicron porosity) is described by an upscaled effective model, while transport in large pores (e.g., microCT resolved porosity) is described by the DFH. The upscaled effective model is derived from the exact DFH equations using asymptotic expansion in respect to small-size characterization parameter. This effective model retains the properties of DFH like chemical and multiphase transport, thus making it applicable to the same range of phenomena as DFH itself. The model is based on the concept that the transport is driven by gradients of chemical potentials of the components present in the mixture. The proposed model would incorporate diffusion transport in addition to pressure-driven transport [12].

Prior to the relative permeability study on the selected reservoir samples, the impact of wettability on imbibition relative permeability was evaluated in a large-scale sensitivity study using an outcrop carbonate rock. In this study sample resided at initial water wet condition with 30° contact angle and using the workflow defined in previous paragraph, digital rock model wettability was modified by changing contact angle at the oil-pore surface contacts to: 30°, 40°, 50°, 60°, 70°, 80°, 100°, 110°, 120°, 130°, 140°, 150° (12 sensitivity runs in total).

Wettability sensitivity was performed by modelling steady-state oil-brine relative permeability imbibition cycle for each wettability state (Figure 8). In 3D Phase saturation figures (at residual oil saturation), water is shown with blue color, oil is shown with red color, and rock is transparent. The simulated flow within the individual 3D saturation models occurs from left to right.

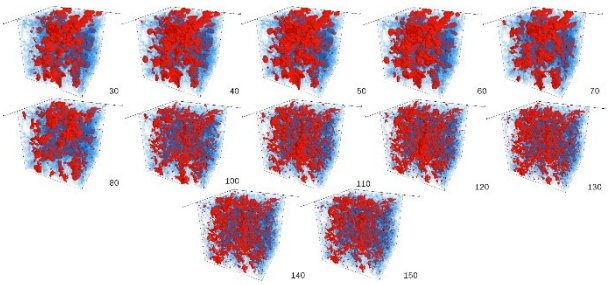

Figure 8. Oil (red) and brine (blue) saturation at the end steady state imbibition cycle for each wettability system with contact angle shown to the right of each respective 3D saturation distribution.

The sensitivity study with DHD simulator allowed us to obtain relative permeability as a function of rock wettability as shown in Figure 9. The results show that as the contact angle increases (from water-wet to oil-wet):

1- The oil mobility is reduced, i.e., oil relative permeability reduces faster as a function of increasing water saturation.
2- The water mobility increases, i.e., the water relative permeability increases faster as a function of increasing water saturation.
3- The water relative permeability end point, $K_{rw}(S_{orw})$, increases.
4- The S_{orw} decreases.

These results are qualitatively agreeable with the expected trend of the relative permeability and residual oil saturation as a function of the wettability of the rock. This test confirms that the DHD model can capture 2 phase flow and can be used for subsequent quantitative prediction of the relative permeability and capillary pressure curves. This also confirms that DRP need wettability distribution as an input as it significantly affects the results, see Masalmeh et. al., 2015 [8].

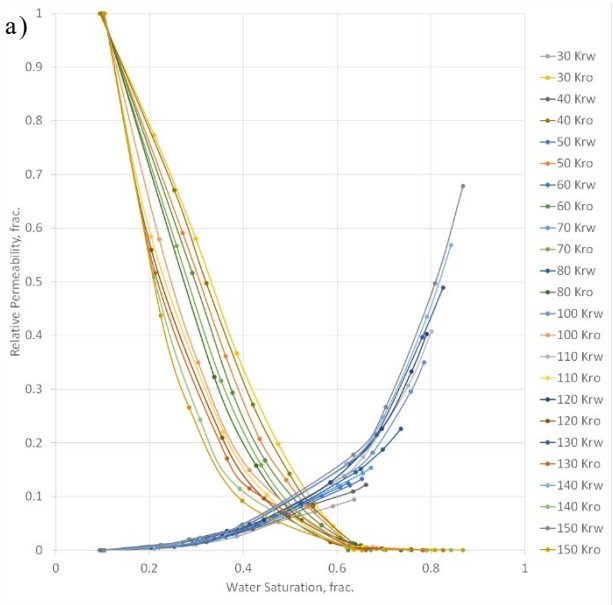

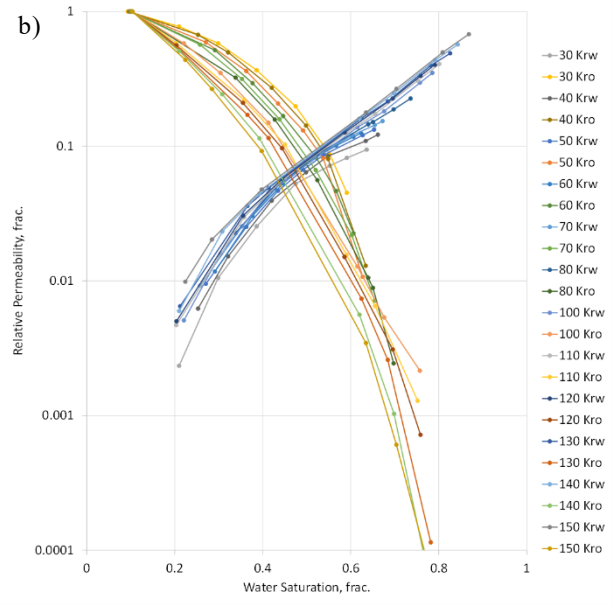

Figure 9. Relative permeability as a function of wettability for studied carbonate outcrop in a) linear scale, b) logarithmic scale.

4.4 Digital results

Waterflood relative permeability curves were predicted in the validated DRMs of samples 18A and 23A with assigned contact angle distribution using the DHD simulator. Fluid data for samples 18A and 23A used in the study is shown in Table 4. Initial water saturation (Swi) was obtained from experimental primary drainage oil-water desaturation test using water-wet porous plate. The Swi values were achieved at the same Pc value, reflecting the respective petrophysical properties of the two samples.

Table 4. Fluid data for samples 18A and 23A.

Parameter/sample ID	18A	23A
Swi Target (frac)	0.045	0.20
Oil viscosity (cP)	2.088	0.562
Oil density (g/cc)	0.828	0.731
Water viscosity (cP)	0.459	0.541
Water density (cP)	1.101	1.148
Interfacial tension (mN/m)	23.96	22.16

To verify sample wettability, the following workflow was implemented: the samples were initially saturated with water. During the multiphase modelling, portions of rock surfaces in contact with oil during the drainage cycle exhibited a change in contact angle to defined value while other surfaces remained at original wetting conditions, rendering samples mixed wet. This distribution of the wettability was made at the end of primary drainage, and was then used in imbibition capillary pressure modelling. Modelling results were compared with experimental drainage and imbibition capillary pressure data of the samples. Figure 10a shows comparison between two imbibition centrifuge Pc measurements with digital simulation of sample #23A. The centrifuge samples have similar properties to sample #23A. The simulation used contact angle value of 105 degrees, which was used for both sample #18A and #23A. Figure 10b shows the primary drainage and imbibition Pc curves for the two samples (the upper limit of the y-axis was set to 10psi only to clearly show the comparison between the two samples). Sample #23A achieved its Swi value at 80psi oil-water Pc. There is no positive part of the imbibition Pc curve because there is no spontaneous imbibition.

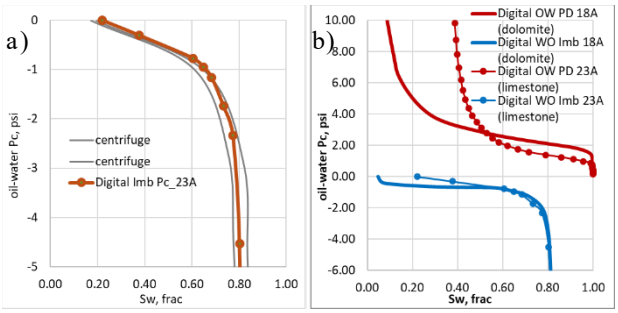

Figure 10. a) Comparison between two imbibition centrifuge Pc measurements and digital simulation of sample #23A. b) Primary drainage and imbibition digital capillary pressure curves for sample 18A and sample 23A.

Once the wettability model was verified, the digital steady-state (SS) oil-brine imbibition relative permeability tests were performed for samples 18A and 23A. Oil and brine were injected into the sample residing at irreducible water saturation Swi. SS digital experiments cover six or more injection ratios (including initial) for imbibition each calculated with the DHD simulator to establish the associated relative permeability points. At each ratio, the injection continues until a two-phase pseudo-equilibrium is established, which is defined as a stabilization of phase saturations, phase production ratios and phase velocities. Once the equilibrium is reached for the current ratio, the digital experiment continues with the next injection ratio and at the final step only brine is injected. The permeability to each phase was determined and recorded as a function of phase saturation and presented in charts. Phase permeability was normalized using absolute brine permeability Kw at 100% water saturation. Table 5 presents the simulated absolute permeability together with endpoint permeability and saturation values.

Table 5. Simulated absolute permeability and endpoint values.

Permeability/Saturation	18A	23A
Kw (mD)	55.36	50.05
Swi (fraction)	0.048	0.220
Kro(Swi)(fraction)	0.752	0.759
Sor (fraction)	0.147	0.135
Krw(Sor) (fraction)	0.483	0.692

Resulting imbibition Kr curves are presented in Figures 11a and 11b for samples 18A and 23A, respectively. The data is plotted in linear scale and semilog scale to properly present the data at the full saturation range.

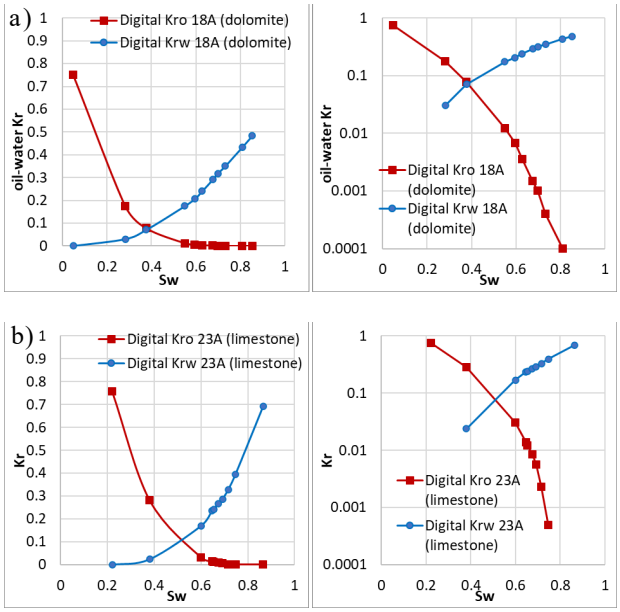

Figure 11. Linear scale (left) and semi log scale (right) relative permeability as a function of water saturation for sample 18A (a) and sample 23A (b).

Oil and brine 3D saturations at Swi and Sor conditions are shown in Figure 12 and 13 for sample 18A and 23A, respectively.

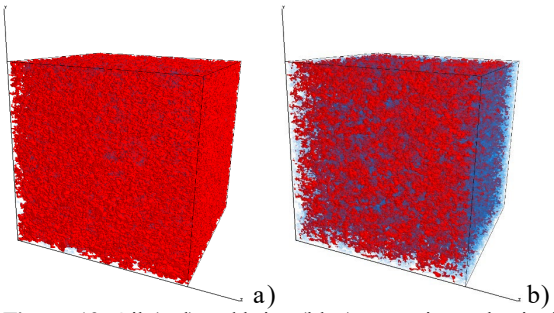

Figure 12. Oil (red) and brine (blue) saturation at beginning (a) and at the end (b) of steady state imbibition cycle for sample 18A.

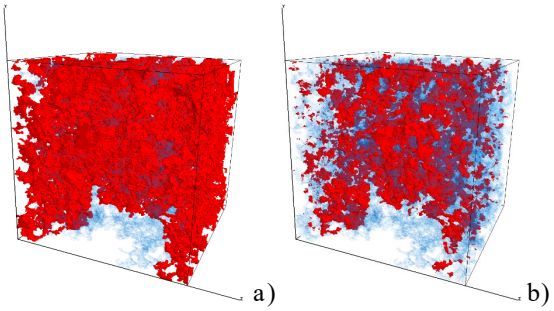

Figure 13. Oil (red) and brine (blue) saturation at beginning (a) and at the end (b) of steady state imbibition cycle for sample 23A.

In 3D phase saturation figures, water is shown with blue color, oil is shown with red color, and rock is transparent. The flow occurs from left to right within individual 3D models.

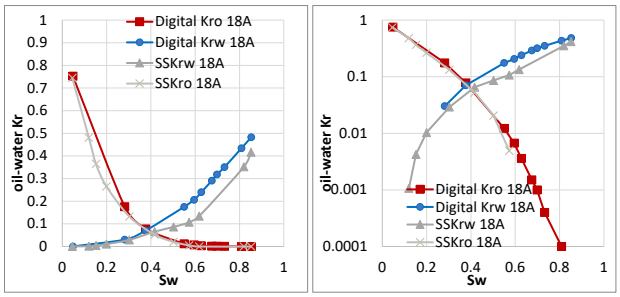

Figure 14. Comparison between physical SSKr and digital Kr curves. Linear scale (left) and semi log scale (right) relative permeability as a function of water saturation for sample 18A.

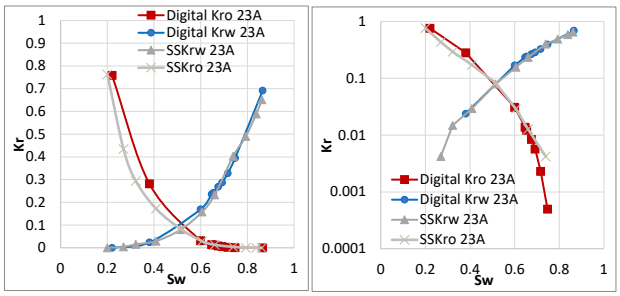

Figure 15. Comparison between physical SSKr and digital Kr curves. Linear scale (left) and semi log scale (right) relative permeability as a function of water saturation for sample 23A.

Figures 14 and 15 show a comparison of the measured and predicted relative permeability curves. Both linear scale and semilog scale are provided to emphasize the similarities between the physical and digital data. The digital curves compared very well with the experimental measurements performed on the corresponding SCAL plugs. The relative permeability end points (both oil and water) agree very well with the measured data, especially for sample 23A. The shape of the relative permeability curves was also well predicted. The physical measurement of the water relative permeability curve for sample 18A may have been influenced by experimental capillary end effect, which will be discussed in the later section.

5 Discussions

Digital SCAL is an important technology for testing two-phase flow behavior using digital models, including oil-water capillary pressure and relative permeability. It provides accelerated analysis that would optimize the time needed for laboratory core analysis experiments. However, it is necessary to ensure that the digital model accurately represents the pore structure and wettability distribution, and that the pore-scale simulation obeys fundamental physics of flow at the pore level.

In this research work, representation of the pore structures in the digital models was confirmed by physical core measurements like rock porosity, permeability and pore-throat size distribution. For wettability representation, we adopted modeling workflows in [8,9], where the advancing contact angle was derived from physical primary drainage and imbibition capillary pressure curves, and by matching digital imbibition curve to measured imbibition Pc curves. The used hybrid protocol

here proved to be a very good approach for the prediction of imbibition relative permeability experiments. It is worth mentioning that it would be ideal if the imbibition capillary pressure curve were measured on the same relative permeability sample for accurate derivation of input contact angle. High-quality integrated SCAL data is essential to guide the DSCAL workflow.

In our case, the contact angle was only predicted from the heterogeneous limestone sample 23A, where imbibition Pc data was available from two sister plugs (figure 10a). Similar contact angle derivation was not possible for the dolomite sample 18A due to the lack of a proper sister plug with good-quality imbibition Pc data. Hence, the same contact angle of 105 degrees was used for both rock types. Anyway, the predicted relative permeability curves from both samples showed very good match with the experimental Kr curves.

Laboratory measurements of relative permeability should be quality checked before it can be used to evaluate fluid flow behavior in the reservoir. For steady state relative permeability, both pressure and saturation raw data should attain stability at each fractional flow rate [10]. Failure to establish equilibrium conditions will result in poor Kr measurements and hence the physical data should not be used to judge digital computations. Figure 16 and 17 show pressure and saturation curves from the waterflood Kr measurements on sample 18A and 23A, respectively. Both samples show high-quality equilibrium pressure data at all fractional flow rates. However, sample 18A suffered from severe capillary end effect starting from 0.5 frac Sw as can clearly be observed from the corresponding in-situ saturation monitoring plot in figure 16. This Pc end effect would lead to a suppression in the Krw curve [11], and hence the possible reason for the mismatch between the physical and digital Krw curves beyond 0.5 frac Sw. This is only a qualitative analysis, and a more detailed investigation of the experimental data including numerical simulation should be done in the future, which may improve the match with the digital Krw curve.

Initial water saturation (Swi) was an input parameter into the DSCAL model as a target saturation to initiate the model at the start of the imbibition simulation. It was constrained by experimental data (i.e., desaturation on the porous plate) to represent initial conditions of the waterflood test. On the other hand, residual oil saturation (Sor) was a simulated parameter at the end of the digital computations based on the pore structure network, wettability and Swi. The pre-assessment computations from Figure 9 serve as evidence supporting validation of the mathematical model used in the DFH method. It is worth mentioning that the Sor from physical Kr measurement of sample 23A (0.138frac) was also confirmed by the sister plug data (0.113frac) from imbibition multi-speed centrifuge experiments (see Figures 10a and 15).

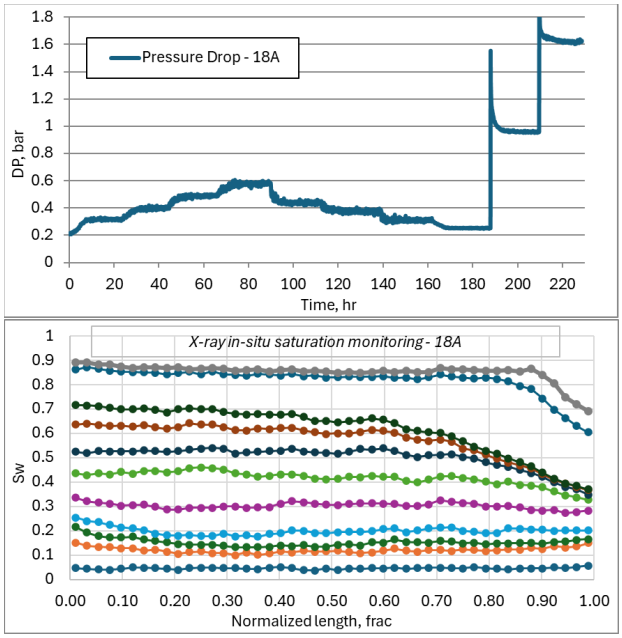

Figure 16. Pressure and saturation profile data – sample 18A.

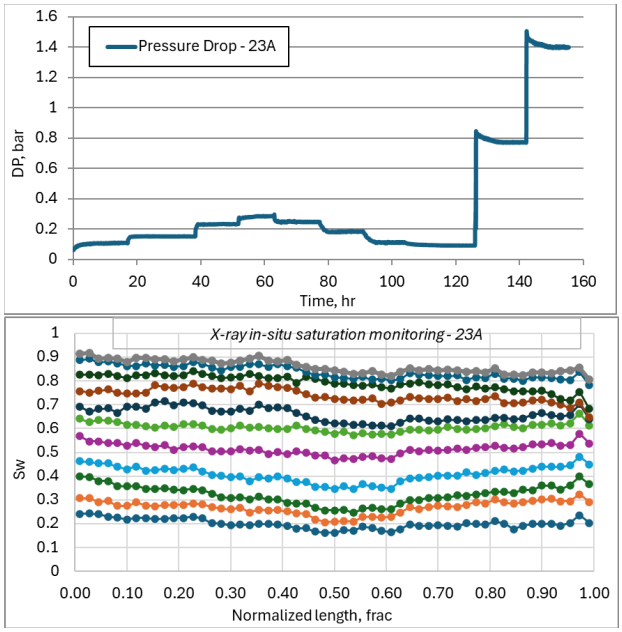

Figure 17. Pressure and saturation profile data – sample 23A.

Both samples 18A and 23A reached almost the same Sor value, although they started from different Swi. This is a clear impact of the different microstructures on the endpoint saturation. Despite similar Sor values, figures 12 and 13 show different 3D phase saturation distributions, which is a direct manifestation of the higher degree of heterogeneity in sample 23A. Figure 18 compares the two Kr data between sample 18A (homogeneous dolomite) and 23A (heterogeneous limestone). The curves show different flow behavior, possibly due to different microstructures because both samples were simulated using the same contact angle.

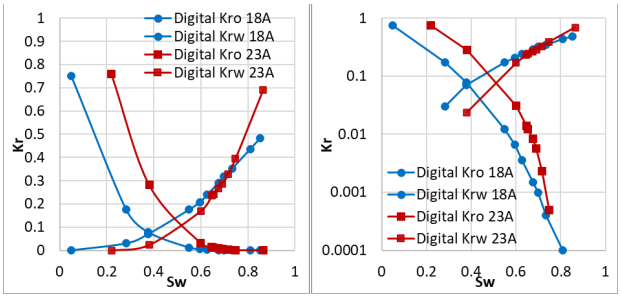

Figure 18. Comparison of the Kr curves between sample 18A and 23A.

6 Summary and Conclusions

This work was part of a validation and verification project to investigate Digital SCAL pore-scale simulations by the DFH method. The study ran on a blind test basis, where experimental relative permeability curves were not disclosed until after the digital results were reported. One homogeneous unimodal dolomite sample and one heterogeneous bimodel limestone sample were selected to undergo DSCAL simulations. The following can be summarized and concluded from the results in this study.

1. Multi-scale microCT and SEM imaging were necessary to accurately represent the microstructures of the reservoir core samples
2. Selection of subsamples and creation of digital rock models were initially guided by plug CT data and were later verified and validated by a hybrid approach based on experimental measurements of plug porosity, absolute permeability and high-pressure mercury injection experiments.
3. Wettability was constrained by experimental measurements of drainage-imbibition Pc curves. Specific advancing contact angle was derived using Masalmeh model [9].
4. Detailed pre-assessment of the DHD computations based on the DFH method revealed simulation results that were in line with expected trends from relative permeability and residual oil saturation as a function of wettability. Such analysis confirmed that the direct modelling method can capture two phase flow and hence can be used for subsequent quantitative prediction of the relative permeability and capillary pressure curves.
5. Digital Kr curves were simulated in the two rock models and compared very well with the experimental steady state relative permeability measurements performed on the corresponding SCAL plugs.

In summary, this study confirms that, in its current state, Digital Rock Physics (DRP) can reliably predict two-phase fluid flow properties when constrained by experimentally derived wettability and contact angle distributions. This underscores the necessity for pore-scale modelling efforts to pivot from attempting *a priori* predictions toward determining the extent of experimental Special Core Analysis (SCAL) and imaging data required to calibrate or constrain models before computing two- or three-phase flow properties for field applications. Such a shift not only enhances the applicability of DRP technology but also fosters greater acceptance and trust within the industry.

The premature introduction of DRP technology approximately two decades ago—as a purported solution for predicting multiphase flow properties based solely on micro-CT images of small rock samples—led to unrealistic expectations. This approach, which often neglected the complexities of wettability and contact angle distribution, among other challenges, resulted in unreliable predictions and subsequent skepticism within the oil industry. By integrating SCAL and imaging data into DRP workflows, we can address these challenges and improve the reliability of DRP prediction capability.

7 Nomenclature

Symbol

Kr	Relative permeability
Kro	Oil relative permeability
Krw	water relative permeability
Kw	Absolute water permeability
Pc	Capillary pressure
Sw	Water saturation
Swi	Initial water saturation
Sor	Residual oil saturation

Abbreviations

AMICS	Advanced Mineral Identification and Characterization System
BSE	Back Scattered Electron
CT	Computed Tomography
DHD	Direct Hydrodynamic
DHF	Density Functional Hydrodynamics
DP	Pressure Drop
DRM	Digital Rock Model
DRP	Digital Rock Physics
DSCAL	Digital SCAL
EDS	Energy Dispersive X-ray Spectroscopy
EOR	Enhanced Oil Recovery
Frac	Fractional
MICP	Mercury Injection Capillary Pressure
RCA	Routine Core Analysis
SCAL	Special core analysis
SEM	Scanning electron microscopy
SS	Steady State
%	Percent

The authors would like to acknowledge ADNOC and SLB Management for the permission to publish the results of this study.

References

1. A. Demianov, O. Dinariev, and N. Evseev, Density Functional Modelling in Multiphase Compositional Hydrodynamics. Canadian Journal of Chemical Engineering **89**: 206–226 (2011).
2. O. Dinariev, A Hydrodynamic Description of a Multicomponent Multiphase Mixture in Narrow Pores and Thin Layers. Journal of Applied Mathematics and Mechanics **59** (5): 745–752 (1995).
3. D. Klemin, A. Serebryanskaya, O. Savelev, et al., Digital Rock Technology Accelerates Carbonate Rock Laboratory Analysis. Presented at the Gas & Oil Technology Showcase and Conference, Dubai, UAE, 21–23 October (2019). SPE-198610-MS. https://doi.org/10.2118/198610-MS.
4. D. Klemin, P. Schlicht, R.E. Distaso, et al., Rigorous Digital Rock Technology Validation Through Cross-Sector Collaboration. Presented at SPE Reservoir Characterization and Simulation Conference and Exhibition, Abu Dhabi, UAE, 24–26 January (2023). SPE-212617-MS. https://doi.org/10.2118/212617-MS.
5. M.R. Dernaika, B. Mansour, M. Konda, D. Klemin R. Bhakta, M.A. Gibrata, Q. Huang, L. Rouis, G. Ameish, and Magdi Eldali, Relative Permeability Measurements Using Different Fluid Systems in an Unconsolidated Sandstone Reservoir, SPE-223478-MS presented at the SPE Caspian Technical Conference and Exhibition (2024)
6. D.L. Zhang, X. Shi, C. Qi, et al., Formation Characterization and Production Forecast of Tight Sandstone Formations in Daqing Oilfield through Digital Rock Technology. Presented at SPE ATCE 2021, Dubai, UAE, 2-23 September (2021). SPE-206055-MS. https://doi.org/10.2118/195872-MS.
7. J. Moreno Ortiz, J. Gossuin, Y. Liu, D. Klemin, O. Gurpinar, T. Gheneim Herrera // Improved Upscaling of EOR Systems for Realistic Reservoir Modeling with the Aid of Multi-Scale Verification, SPE-195872, SPE ATCE, 30 September - 2 October 2019, Calgary, Alberta, Canada
8. S.K. Masalmeh, X. Jing, S. Roth, C. Wang, H. Dong, and M. Blunt, Towards Predicting Multi-Phase Flow in Porous Media Using Digital Rock Physics: Workflow to Test the Predictive Capability of Pore-Scale Modeling. SPE-177572-MS presented at the Abu Dhabi International Petroleum Exhibition and Conference held in Abu Dhabi, UAE, 9–12 November (2015).
9. S.K. Masalmeh, and X.D. Jing, Improved Characterisation and Modelling of Carbonate Reservoirs for Predicting Waterflooding Performance", SPE paper 11722_PP, presented at the International Petroleum Technology Conference held in Dubai, U.A.E., December 4–6 (2007).
10. S.K. Masalmeh, and X.D. Jing, The Importance of Special Core Analysis in Modelling Remaining Oil Saturation in Carbonate Fields, SCA-2008-03 (2008)
11. M.R. Dernaika, M.Z. Kalam, M.A. Basioni, S.M. Skjæveland, Hysteresis of Capillary Pressure, Resistivity Index and Relative Permeability in Different Carbonate Rock Types, Petrophysics, **53**, 5 (2012)
12. O. Dinariev, N. Evseev, D. Klemin, Density Functional Hydrodynamics in Multiscale Pore Systems: Chemical Potential Drive, E3S Web of Conferences 146, 01001 (2020), SCA2019-002. https://doi.org/10.1051/e3sconf/202014601001